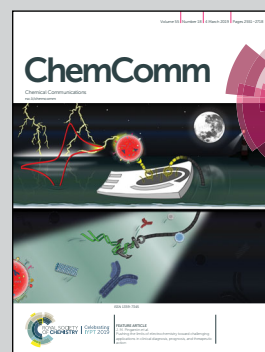


Showcasing research from Professor Wei Lu's group from the Department of Mechanical Engineering at the University of Michigan, Ann Arbor, United States.

Highly ambient-stable few-layer black phosphorene by pulsed laser exfoliation and HEMM

Pulsed laser exfoliation of black phosphorus powders and crystals synthesized with high energy mechanical milling (HEMM) enables production of highly ambient-stable few-layer black phosphorene.

As featured in:



See Wei Lu *et al.*,
Chem. Commun., 2019, 55, 2601.



Cite this: *Chem. Commun.*, 2019, 55, 2601

Received 18th November 2018,
Accepted 2nd January 2019

DOI: 10.1039/c8cc09174a

rsc.li/chemcomm

Highly ambient-stable few-layer black phosphorene by pulsed laser exfoliation and HEMM

Jianyu Zhang,  Hosop Shin  † and Wei Lu  *

Pulsed laser exfoliation was successfully applied to fabricate few-layer phosphorene from high energy mechanical milling (HEMM) synthesized black phosphorus (BP) powders and crystals. The results show that the polycrystalline phosphorene laser-exfoliated from the HEMM-synthesized BP powders is highly stable in ambient environments, providing proof-of-concept for the low-cost fabrication of highly stable few-layer phosphorene for large-scale applications.

Black phosphorus (BP) is the most thermodynamically stable phosphorus allotrope, from both experimental and quantum chemical perspectives.^{1,2} It can be synthesized by the high pressure method, chemical vapor deposition (CVD) and mineralization.^{3,4} Phosphorene, a two-dimensional monolayer or few-layer BP, has recently attracted attention due to its unique structure containing puckered individual layers connected by weak van der Waals forces, as well as superior electronic and optoelectronic properties.^{5,6} Phosphorene possesses wide and tunable bandgaps from 0.3 eV to 1.5 eV in an inverse relationship to its thickness. This property makes phosphorene a promising material for use in digital devices alongside graphene and other transition metal materials.⁷ In addition, a high carrier mobility (286–1000 cm² V⁻¹ s⁻¹),^{8,9} anisotropic in-plane transport properties and a high on–off current ratio (10²–10⁵) render phosphorene a suitable channel material for field effect transistors.¹⁰ BP and phosphorene are both promising candidates for use as high-capacity anode materials (2596 mA h g⁻¹) for lithium-ion battery applications,^{11,12} whose capacity is much higher than that of the commonly used graphite (372 mA h g⁻¹). It is of importance to note that both materials can be used in sodium-ion (Na-ion) batteries, where graphite is not applicable.^{13,14} Similar to other high-capacity anode materials such as silicon, however, BP-based Li-ion/Na-ion batteries suffer from rapid capacity fade, mainly owing to large volume expansion and subsequent structural failure.¹⁵

According to *in situ* transmission electron microscopy (TEM) studies, phosphorene is more robust during lithiation/delithiation or sodiation/desodiation in comparison to bulk BP particles.^{16,17} Thus, phosphorene-based anode materials have been proposed to mitigate significant volume expansion and contraction (370% in a Li-ion battery, 500% in a Na-ion battery).^{18,19} Multiple strategies have been used to exfoliate phosphorene. Mechanical cleavage through scotch-tape produces the highest quality samples, but productivity is low. Liquid-phase exfoliation assisted by ion intercalation, ultra-sonication and shear force is a more scalable process. An appropriate processing time, power and centrifugation parameters are necessary to control phosphorene thickness and size distribution.^{20,21} Unfortunately, phosphorene is known for its fast degradation within hours of exposure to ambient environments,²² especially when oxygen, moisture and light are involved together.^{23–25} Significant compositional and structural changes will result in a loss of phosphorene's electronic and physical properties. Many strategies have been explored to address this issue. Graphene, boron nitride and Al₂O₃ have been used to encapsulate phosphorene and prevent air contamination.^{26–28} A study on fluorinated phosphorene has reported that the lifetime of phosphorene extends up to 7 days without an additional passivation layer.²⁹ Recently, Ag⁺ modified BP was found to exhibit better stability and transistor performance.³⁰ However, it should be noted that the current phosphorene-based battery research relies on single-crystalline bulk phosphorus,^{18,19} which requires stringent synthesis conditions and is cost-prohibitive. Both degradation and high costs have hindered the industry-scale applications of phosphorene in batteries and other fields.

In this work, we present a cost-effective and easy-to-implement technique to exfoliate phosphorene with a pulsed laser using high energy mechanical milling (HEMM)-synthesized BP powder as the precursor. Surprisingly, the as-exfoliated phosphorene from the HEMM-synthesized BP powder was found to exhibit excellent ambient stability compared to that exfoliated from bulk BP crystals, as characterized by TEM and Raman spectroscopy.

BP is not naturally available and must be transformed from red phosphorus or white phosphorus under high pressure and

Department of Mechanical Engineering, University of Michigan, Ann Arbor, Michigan, 48109, USA. E-mail: weilu@umich.edu

† Current address: Department of Mechanical and Energy Engineering, Indiana University-Purdue University Indianapolis, Indianapolis, IN 46202, USA.

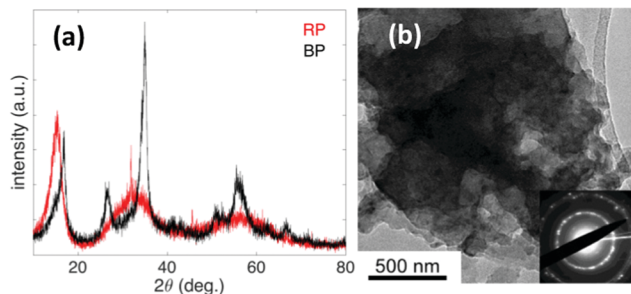


Fig. 1 (a) X-ray diffraction patterns of black phosphorus (BP) and red phosphorus (RP); (b) TEM image of the HEMM-synthesized bulk BP with the corresponding SAED pattern.

high temperature conditions.^{31,32} HEMM is a scalable method for creating the appropriate conditions for producing BP.¹¹ To obtain the raw BP powder, 6 g of red phosphorus (98.9%, Alfa Aesar) was mixed with stainless steel balls (12.7 mm ball: 10EA + 9.5 mm ball: 17EA) inside a stainless steel vessel with a capacity of 50 mL. The vessel was sealed in an argon-filled glovebox with the O₂ and H₂O levels maintained lower than 1 ppm. A shaker miller (8000M Mixer/Mill, SPEX) performed HEMM for 6 h. Red phosphorus was transformed to black phosphorus as shown in the XRD pattern in Fig. 1a. From the TEM image with the SAED pattern in Fig. 1b, we can observe thick BP stacks with a polycrystalline structure. The puckered layered structure indicates the potential to be further exfoliated into phosphorene.

The as-synthesized BP powder was then added into *N*-methyl-2-pyrrolidone (NMP, Alfa Aesar, 99.5%) in a vial. The sample solution was sealed with a cap attached with a sapphire window in a glovebox to prevent oxidation. An Nd-YAG pulsed laser with a wavelength of 1064 nm and a single pulse energy output of 100 mJ was used to scan the target through the window at a frequency of 1 Hz for 4 h. Each single pulse was less than 50 μs in duration. A magnetic stirrer was used for continuous mixing of the solution at 1000 rpm to ensure homogenous processing. After laser-induced exfoliation, the mixture was statically stored in the glovebox for 12 h. The upper 2/3 of the supernatant was then collected and centrifuged at 3000 rpm for 30 min to remove large unexfoliated BP particles. The collected supernatant was centrifuged again at 9000 rpm for 30 min. The final phosphorene deposit (denoted as HEMM phosphorene) was rinsed with ethanol several times to remove the NMP residue, and then dried on an SiO₂ (200 nm)/Si substrate in a vacuum for 12 h. In Fig. 2a, the atomic force microscopy (AFM) image and the corresponding height profile indicate an average size of about 1–2 μm and an average height of about 6 nm. We demonstrated for the first time that six-to-nine-layer phosphorene could be successfully exfoliated using HEMM-synthesized BP powder. Considering the simplicity of HEMM and the abundance of phosphorus, the proposed method could be easily scaled up for industrial production of phosphorene. In addition, a pulsed laser is energy-efficient and tunable; the average power during the process was only 0.1 W. By optimizing the focal point of the laser beam and the power, phosphorenes with different sizes and thicknesses can be obtained.

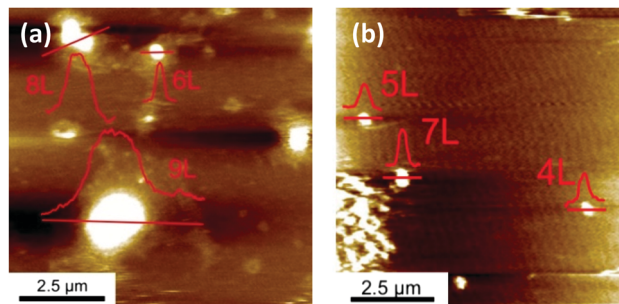


Fig. 2 AFM topography of the (a) phosphorene laser-exfoliated from the HEMM-synthesized BP powder (HEMM phosphorene) and (b) phosphorene laser-exfoliated from a BP crystal (basic phosphorene).

For comparison, a bulk BP crystal (99.998%, Sigma-Aldrich) was also used to exfoliate phosphorene (denoted as basic phosphorene) in NMP by pulsed laser using the same procedure. The AFM image and the height profile of the basic phosphorene in Fig. 2b show fewer layers and smaller sizes compared to that of the HEMM phosphorene. We suspect that the HEMM-synthesized powder may be composed of loosely connected phosphorene bundles, which makes it easier for large flakes to exfoliate. In contrast, it would be more difficult to peel off phosphorene from a BP crystal, leading to smaller phosphorene pieces. More importantly, TEM and Raman characterization experiments show that the HEMM phosphorene exhibit superior ambient stability compared with the basic phosphorene, which is discussed in further detail below.

The dried HEMM phosphorene and basic phosphorene were transferred onto a copper grid with a perforated carbon membrane for TEM analysis. Measurements were performed using a JEOL JEM-2010 TEM at a voltage of 200 keV. As shown in Fig. 3a and c, the initial as-exfoliated phosphorene morphologies are quite different from one another. HEMM phosphorene presents a corrugated surface with more bends, overlaps and wrinkles, mainly because the HEMM process is stochastic in nature. As the high pressure and high temperature required for the transformation of red phosphorus to black phosphorus are obtained by random collision, the synthesized BP and the exfoliated HEMM phosphorene do not show a well-organized, single crystalline layered pattern, but instead show a polycrystalline structure. This structure is revealed by the diffraction rings in the selected area electron diffraction (SAED) pattern in the inset of Fig. 3a. Compared with the exfoliated HEMM phosphorene, the basic phosphorene maintained a flat surface and a single crystalline structure (Fig. 3c).

Phosphorene is known to suffer from rapid degradation when exposed to oxygen and moisture. Previous studies have suggested that complex P_xO_y and phosphoric acid are generated on the surface of phosphorene within a few hours,^{22,24} rendering phosphorene use in general ambient environments impractical. To date, no report on the stability of exfoliated HEMM phosphorene has been published. We exposed our grids with HEMM phosphorene and basic phosphorene to air for 24 h, during which the temperature was constant at 22 °C, and the humidity was between 25 and 30%.

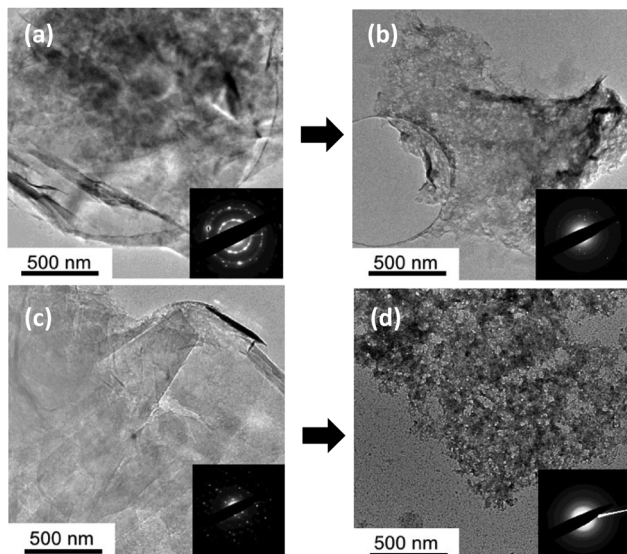


Fig. 3 TEM images with the corresponding SAED patterns of the (a) as-exfoliated HEMM phosphorene, (b) HEMM phosphorene after 24 h air exposure, (c) as-exfoliated basic phosphorene, and (d) basic phosphorene after 24 h air exposure.

TEM analysis revealed obvious morphological changes after this exposure (Fig. 3b and d). Specifically, the surface of the HEMM phosphorene sample became slightly rougher without significant degradation. The SAED pattern also confirmed that the polycrystalline structure was maintained to a certain extent. In contrast, the smooth surface of the basic phosphorene became significantly degraded and contaminated. Such defects and fractures on the surface indicate significant oxidation and dampening, resulting from phosphorene's hygroscopic properties, and indeed, the SAED pattern revealed that the basic phosphorene completely lost its crystalline structure.

To further confirm the different degradation trends, a WITec alpha300 RA confocal Raman system with a laser wavelength of 532 nm was used to analyze the samples. The power was adjusted to less than 0.5 mW with an accumulation time of 30 s to avoid laser-introduced damage during Raman characterization. We maintained a constant level of laser power across all characterization experiments. The magnification of the objective lens was 100 \times and zoomed to an area with a diameter of less than 1 μ m. As mentioned earlier, the samples were stored in air at a temperature of 22 $^{\circ}$ C and humidity ranging from 25 to 30%. Fig. 4 shows the Raman spectra of HEMM phosphorene and basic phosphorene on the SiO₂/Si substrate as a function of storage time. Compared with the bulk BP, all three-vibrational peaks show a slight shift to the right. Monolayer phosphorene is known to have the most significant shift; more layers correspond to a small shift.^{6,33} The minor peak shifts of both the HEMM phosphorene and the basic phosphorene with respect to the bulk BP indicate that the pulsed laser exfoliation of BP produces few-layer phosphorene instead of a single layer one, which is consistent with the AFM and TEM results in Fig. 1–3. Fig. 4a shows a minor decrease in the intensities of the three peaks of HEMM phosphorene during 6 hours of air exposure, as a result of the reaction with the

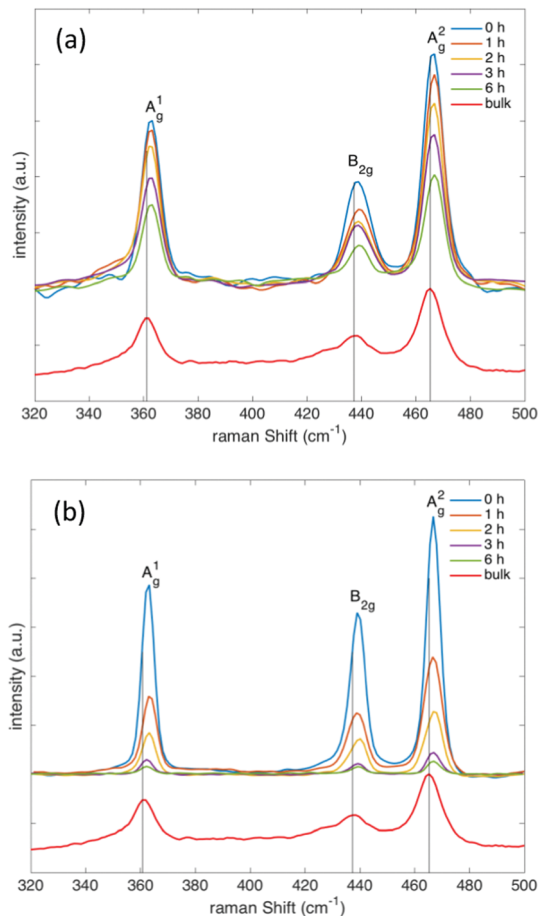


Fig. 4 Raman spectra of (a) HEMM phosphorene and (b) basic phosphorene after exposure to air for 0 h, 1 h, 2 h, 3 h and 6 h. The Raman spectrum of the HEMM-synthesized bulk BP is shown as a reference (red line).

oxygen and water in air. In contrast, the three peaks of the basic phosphorene almost completely disappear during 6 hours of air exposure, indicating significant structural degradation.

Based on these observations, we propose that the following factors may contribute to the superior stability of HEMM phosphorene.

First, the superior stability of HEMM phosphorene is attributed to its morphological and structural characteristics. The average size and thickness of HEMM phosphorene are larger than those of basic phosphorene, and HEMM phosphorene retains a polycrystalline structure rather than a single crystal structure. These characteristics are beneficial in preventing phosphorene degradation, which occurs in a layer-by-layer fashion. A recent study has demonstrated that a larger-sized phosphorene sample degrades more slowly than smaller-sized ones, and the degradation predominantly occurs on the edges rather than in the basal plane.²⁷ Thus, few-layer phosphorene with a perfect layer-by-layer stack and clear edge planes is more susceptible to degradation. We found that HEMM phosphorene has a pseudo-2D polycrystalline structure rather than being a perfect layer-by-layer stack connected by weak van der Waals forces. The randomly distributed crystallized clusters strengthen the cross-layer connection, which may cause HEMM

phosphorene to lack clear edges and boundaries for degradation initialization. Thus, HEMM phosphorene can better withstand damage caused by oxidation.

Second, HEMM phosphorene may have a better NMP-based solvation shell to shield itself from reacting with oxygen. Phosphorene is known to be hydrophilic. Compared with the smooth surface of regular phosphorene, the rough surface of HEMM phosphorene allows it to be effectively covered with an NMP-based solvation shell during the process of liquid-based exfoliation. This shell could enable high oxidative stability. A previous study showed that various solvents are able to form tightly packed solvation shells adjacent to phosphorene surfaces, offering excellent protection from oxygen and water.³⁴

Finally, liquid phase pulsed laser exfoliation intrinsically ensured that the exfoliation occurs locally and quickly to avoid the oxidation conditions during the exfoliation process. In contrast, sonication, another liquid-based exfoliation method, causes both temperature increase and gas leakage as a result of the required long processing time. The uncontrolled temperature increase and vibration-induced gas leakage could accelerate phosphorene degradation. The pulsed laser-based method can prevent these issues.

In summary, we have demonstrated that liquid phase pulsed laser exfoliation combined with HEMM produced a pseudo-2D phosphorene structure that exhibited high stability under ambient conditions. To overcome the issues of phosphorene oxidation and instability, it is necessary to not only avoid oxidation-favorable conditions during exfoliation but also design a phosphorene structure and morphology that impede oxidation. We suggest that 3D-like or pseudo-2D phosphorene with fewer edge planes and a passivation layer is highly desirable for enhancing the long-term resistance to oxidation.

We have proposed a scalable and inexpensive method for fabricating few-layer phosphorene by exfoliation with HEMM-synthesized bulk BP and pulsed laser processing. We found that the exfoliated HEMM phosphorene exhibits superior ambient stability, as confirmed by TEM and Raman characterization experiments. The ease and low cost of processing and the high stability of the produced phosphorene are important for industrial applications, especially in the field of batteries.

This research was supported by the SAMSUNG Global Research Outreach (GRO) Program. The authors gratefully acknowledge the support.

Conflicts of interest

There are no conflicts to declare.

Notes and references

- 1 R. W. Keyes, *Phys. Rev.*, 1953, **92**, 580–584.
- 2 T. Nilges, P. Schmidt and R. Wehrich, in *Encyclopedia of Inorganic and Bioinorganic Chemistry*, Wiley, Hoboken, 2018.
- 3 V. Eswaraiyah, Q. S. Zeng, Y. Long and Z. Liu, *Small*, 2016, **12**, 3480–3502.
- 4 S. Lange, P. Schmidt and T. Nilges, *Inorg. Chem.*, 2007, **46**, 4028–4035.
- 5 R. A. Doganov, E. C. T. O'Farrell, S. P. Koenig, Y. T. Yeo, A. Ziletti, A. Carvalho, D. K. Campbell, D. F. Coker, K. Watanabe, T. Taniguchi, A. H. C. Neto and B. Ozyilmaz, *Nat. Commun.*, 2015, **6**, 7.
- 6 Z. N. Guo, H. Zhang, S. B. Lu, Z. T. Wang, S. Y. Tang, J. D. Shao, Z. B. Sun, H. H. Xie, H. Y. Wang, X. F. Yu and P. K. Chu, *Adv. Funct. Mater.*, 2015, **25**, 6996–7002.
- 7 L. K. Li, J. Kim, C. H. Jin, G. J. Ye, D. Y. Qiu, F. H. da Jornada, Z. W. Shi, L. Chen, Z. C. Zhang, F. Y. Yang, K. Watanabe, T. Taniguchi, W. Ren, S. G. Louie, X. H. Chen, Y. B. Zhang and F. Wang, *Nat. Nanotechnol.*, 2017, **12**, 21–25.
- 8 H. Liu, A. T. Neal, Z. Zhu, Z. Luo, X. F. Xu, D. Tomanek and P. D. Ye, *ACS Nano*, 2014, **8**, 4033–4041.
- 9 L. K. Li, Y. J. Yu, G. J. Ye, Q. Q. Ge, X. D. Ou, H. Wu, D. L. Feng, X. H. Chen and Y. B. Zhang, *Nat. Nanotechnol.*, 2014, **9**, 372–377.
- 10 F. N. Xia, H. Wang and Y. C. Jia, *Nat. Commun.*, 2014, **5**, 6.
- 11 C. M. Park and H. J. Sohn, *Adv. Mater.*, 2007, **19**, 2465–2468.
- 12 J. Sun, G. Y. Zheng, H. W. Lee, N. Liu, H. T. Wang, H. B. Yao, W. S. Yang and Y. Cui, *Nano Lett.*, 2014, **14**, 4573–4580.
- 13 T. Ramireddy, T. Xing, M. M. Rahman, Y. Chen, Q. Dutercq, D. Gunzelmann and A. M. Glushenkov, *J. Mater. Chem. A*, 2015, **3**, 5572–5584.
- 14 X. Liu, Y. W. Wen, Z. Z. Chen, B. Shan and R. Chen, *Phys. Chem. Chem. Phys.*, 2015, **17**, 16398–16404.
- 15 M. Dahbi, N. Yabuuchi, M. Fukunishi, K. Kubota, K. Chihara, K. Tokiwa, X. F. Yu, H. Ushiyama, K. Yamashita, J. Y. Son, Y. T. Cui, H. Oji and S. Komaba, *Chem. Mater.*, 2016, **28**, 1625–1635.
- 16 F. Xu, H. Y. Ma, S. Y. Lei, J. Sun, J. Chen, B. H. Ge, Y. M. Zhu and L. T. Sun, *Nanoscale*, 2016, **8**, 13603–13610.
- 17 F. Xu, B. H. Ge, J. Chen, A. Nathan, L. H. L. Xin, H. Y. Ma, H. H. Min, C. Y. Zhu, W. W. Xia, Z. R. Li, S. L. Li, K. H. Yu, L. J. Wu, Y. P. Cui, L. T. Sun and Y. M. Zhu, *2D Mater.*, 2016, **3**, 12.
- 18 J. Sun, H. W. Lee, M. Pasta, H. T. Yuan, G. Y. Zheng, Y. M. Sun, Y. Z. Li and Y. Cui, *Nat. Nanotechnol.*, 2015, **10**, 980–985.
- 19 Y. Zhang, H. W. Wang, Z. Z. Luo, H. T. Tan, B. Li, S. N. Sun, Z. Li, Y. Zong, Z. C. J. Xu, Y. H. Yang, K. A. Khor and Q. Y. Yan, *Adv. Energy Mater.*, 2016, **6**, 9.
- 20 M. Qiu, Z. T. Sun, D. K. Sang, X. G. Han, H. Zhang and C. M. Niu, *Nanoscale*, 2017, **9**, 13384–13403.
- 21 S. C. Dhanabalan, J. S. Ponraj, Z. N. Guo, S. J. Li, Q. L. Bao and H. Zhang, *Adv. Sci.*, 2017, **4**, 32.
- 22 W. Luo, D. Y. Zemlyanov, C. A. Milligan, Y. C. Du, L. M. Yang, Y. Q. Wu and P. D. Ye, *Nanotechnology*, 2016, **27**, 10.
- 23 S. Walia, Y. Sabri, T. Ahmed, M. R. Field, R. Ramanathan, A. Arash, S. K. Bhargava, S. Sriram, M. Bhaskaran, V. Bansal and S. Balendran, *2D Mater.*, 2017, **4**, 8.
- 24 G. X. Wang, W. J. Slough, R. Pandey and S. P. Karna, *2D Mater.*, 2016, **3**, 7.
- 25 J. O. Island, G. A. Steele, H. S. J. van der Zant and A. Castellanos-Gomez, *2D Mater.*, 2015, **2**, 6.
- 26 A. Avsar, I. J. Vera-Marun, J. Y. Tan, K. Watanabe, T. Taniguchi, A. H. C. Neto and B. Ozyilmaz, *ACS Nano*, 2015, **9**, 4138–4145.
- 27 J. S. Kim, Y. N. Liu, W. N. Zhu, S. Kim, D. Wu, L. Tao, A. Dodabalapur, K. Lai and D. Akinwande, *Sci. Rep.*, 2015, **5**, 7.
- 28 C. Y. Xing, G. H. Jing, X. Liang, M. Qiu, Z. J. Li, R. Cao, X. J. Li, D. Y. Fan and H. Zhang, *Nanoscale*, 2017, **9**, 8096–8101.
- 29 X. Tang, W. Y. Liang, J. L. Zhao, Z. J. Li, M. Qiu, T. J. Fan, C. S. Luo, Y. Zhou, Y. Li, Z. N. Guo, D. Y. Fan and H. Zhang, *Small*, 2017, **13**, 10.
- 30 Z. N. Guo, S. Chen, Z. Z. Wang, Z. Y. Yang, F. Liu, Y. H. Xu, J. H. Wang, Y. Yi, H. Zhang, L. Liao, P. K. Chu and X. F. Yu, *Adv. Mater.*, 2017, **29**, 8.
- 31 P. W. Bridgman, *J. Am. Chem. Soc.*, 1914, **36**, 1344–1363.
- 32 S. Endo, Y. Akahama, S. Terada and S. Narita, *Jpn. J. Appl. Phys.*, 1982, **21**, L482–L484.
- 33 W. L. Lu, H. Y. Nan, J. H. Hong, Y. M. Chen, C. Zhu, Z. Liang, X. Y. Ma, Z. H. Ni, C. H. Jin and Z. Zhang, *Nano Res.*, 2014, **7**, 853–859.
- 34 D. Hanlon, C. Backes, E. Doherty, C. S. Cucinotta, N. C. Berner, C. Boland, K. Lee, A. Harvey, P. Lynch, Z. Gholamvand, S. F. Zhang, K. P. Wang, G. Moynihan, A. Pokle, Q. M. Ramasse, N. McEvoy, W. J. Blau, J. Wang, G. Abellan, F. Hauke, A. Hirsch, S. Sanvito, D. D. O'Regan, G. S. Duesberg, V. Nicolosi and J. N. Coleman, *Nat. Commun.*, 2015, **6**, 11.